Biosensors and Bioelectronics 225 (2023) 115089

Contents lists available at ScienceDirect

Biosensors and Bioelectronics

journal homepage: www.elsevier.com/locate/bios

High-throughput co-culture system for analysis of spatiotemporal cell-cell signaling

Minjun Son [a,b,*,1], Andrew G. Wang [a,c,1], Emma Kenna [a], Savaş Tay [a,b,**]

[a] Pritzker School of Molecular Engineering, University of Chicago, Chicago, IL, 60637, USA
[b] Institute for Genomics and Systems Biology, University of Chicago, Chicago, IL, 60637, USA
[c] Medical Scientist Training Program, University of Chicago, Chicago, IL, 60637, USA

ARTICLE INFO

Keywords:
Microfluidics
Cell-to-Cell signaling
Spatiotemporal analysis
NF-κB
Inflammatory signaling

ABSTRACT

Study of spatial and temporal aspects of signaling between individual cells is essential in understanding development, the immune response, and host-pathogen interactions. We present an automated high-throughput microfluidic platform that chemically stimulates immune cells to initiate cytokine secretion, and controls the formation of signal gradients that activate neighboring cell populations. Furthermore, our system enables controlling the cell type and density based on distance, and retrieval of cells from different regions for gene expression analysis. Our device performs these tasks in 192 independent chambers to simultaneously test different co-culture conditions. We demonstrate these capabilities by creating various cellular communication scenarios between macrophages and fibroblasts *in vitro*. We find that spatial distribution of macrophages and heterogeneity in cytokine secretion determine spatiotemporal gene expression responses. Furthermore, we describe how gene expression dynamics depend on a cell's distance from the signaling source. Our device addresses key challenges in the study of cell-to-cell signaling, and provides high-throughput and automated analysis over a wide range of co-culture conditions.

1. Introduction

Tissues consist of a mixture of specialized cell types that are spatially organized and communicate via secreted signaling molecules. Individual cells within tissue reside in a dense and heterogeneous physical environment, which affects the diffusion of secreted molecules, metabolites, and even dissolved gases (Josan et al., 2012; Kumar et al., 2019; Oyler-Yaniv et al., 2017). As a result, these molecules form spatial gradients where the local signal concentration rapidly change across space. The diffusivity of signaling molecules is also determined by their physical and chemical properties such as polarity, concentration, or mass (Madura et al., 1995). Modeling and *in vitro* study of these resultant signaling gradients and their effects on cellular response is necessary for a proper understanding of collective cell behavior (Ellison et al., 2016; Mugler et al., 2016).

Signals from a small number of cells can induce population-wide responses. For example, damage signals from a small population of injured cells rapidly propagate to activate wound healing responses over a large area (Handly et al., 2015; Handly and Wollman, 2017) or induce local apoptosis in tissue (Riegman et al., 2019). A single infected cell or activated sentinel cell can trigger or suppress broader inflammatory response (Avraham et al., 2015; Neupane et al., 2020; Shalek et al., 2014; Son et al., 2022; Xue et al., 2015). Furthermore, morphogen gradients produced by localized groups of cells control development of organs, limbs, and intra-organ structures (Christian, 2012; Durrieu et al., 2018; Zinski et al., 2017). Quorum-sensing molecules secreted by single bacteria or subpopulations can diffuse and coordinate population level responses like biofilm formation and swarming (Daniels et al., 2004; Parsek and Greenberg, 2005; Zhou et al., 2020).

Despite the importance of individual cell responses and their spatial and temporal characteristics, the majority of cell signaling research has used population-level responses to well-mixed stimuli, due to technical limitations in generating, controlling and measuring single cell responses with sufficient spatial and temporal resolution. This approach fails to capture local production and consumption of signaling molecules and its effect on cellular decision-making. Accurate study of cellular

* Corresponding author. Pritzker School of Molecular Engineering, University of Chicago, Chicago, IL, 60637, USA.
** Corresponding author. Institute for Genomics and Systems Biology, University of Chicago, Chicago, IL, 60637, USA.
E-mail addresses: dr.minjunson@gmail.com (M. Son), tays@uchicago.edu (S. Tay).
[1] These authors contributed equally: Minjun Son, Andrew Wang.

https://doi.org/10.1016/j.bios.2023.115089
Received 13 October 2022; Received in revised form 17 January 2023; Accepted 18 January 2023
Available online 30 January 2023

signaling requires developing novel approaches that reproduce spatio-temporal communication between cells, track signaling responses in single cells, and produce spatially resolved measurements of phenotypic difference due to signaling.

Microfluidics enables precise and adaptable liquid handling and presents a powerful platform for studying cell-cell communication involving diffusion of secreted signals. Previous microfluidic designs created signal gradients over a cell population for the study of chemotaxis and cell to cell communication (Ambravaneswaran et al., 2010; Chang et al., 2014; Englert et al., 2009; Frank and Tay, 2015; Hind et al., 2018; Selimović et al., 2011). However, these designs were limited by low throughput, fixed cellular distributions, and did not have the ability to study gene expression in a spatially resolved manner. Recently, we used a device which enabled studying regional gene expression during inflammatory signaling over space, but the previous designs still remained low-throughput and was unable to control cell type and density effectively (Son et al., 2022).

In this study, we present an automated high-throughput co-culture device and integrated live-cell imaging system for spatiotemporal study of cell signaling. This system controls the communication between two cell populations, generates diffusion-mediated signaling gradients, isolates cells based on location, and controls regional cell distribution and density (cell patterning). These functions can be performed simultaneously in 192 samples with up to 96 unique stimulus conditions. Using this device, we study how heterogeneity of macrophage cytokine secretion affects the responses in neighboring fibroblasts, how distance from a signaling source affects gene expression, and how fibroblast response depends on local macrophage densities.

2. Material and methods

2.1. Microfluidic device design and mold fabrication

The device uses two-layer microfluidics for valve control (Unger et al., 2000), which is highly multiplexed for increased throughput and functional control of the device. The chip design was drawn using AutoCAD®, and was fabricated using conventional soft-lithography process (Gomez-Sjoberg et al., 2010; Son et al., 2021). More details about the design and the fabrication process can be found in the supplemental information.

2.2. Microfluidic device fabrication

The microfluidic device was fabricated using the same protocol as described in our previous study (Son et al., 2021). For the thin PDMS layer with fluid layer features, ~10 g of mixture was poured on the fluid mold (pretreated with chlorotrimethylsilane) and was spun at 2,300 RPM to generate ~ 50 μm height PDMS layer. After curing, this thin layer was aligned with the thick PDMS slab that has control features using a custom stereomicroscope with a XYZ translation stage. After punching holes and cleaning, the PDMS layers were bonded to a large glass substrate (127.8 x 85.5 × 1 mm, Marienfeld). All layers and substrates were bonded using oxygen plasma (Harrick, PDC-001).

2.3. Cell culturing and media

RelA$^{-/-}$ RelA-DsRed NIH3T3 mouse embryonic fibroblasts (3T3s) were cultured in DMEM high glucose (Gibco) supplemented with 10% fetal bovine serum (Omega Scientific), 2 mM GlutaMAX (Gibco), and 1% penicillin/streptomycin (Lonza). 3T3s were resuspended at 5*10^5 cells/mL for loading the microfluidic device. Details for isolating and culturing primary murine fibroblast and macrophage (RAW264.7 and BMMΦ) are described in supplemental information.

2.4. Experiment preparation and procedure

Prior to the experiment, the 88 control inputs in the device (Fig. S1) were connected to solenoid valves (Festo, 197334) through Tygon tubes (Cole-Parmer, ND-100-80). Each solenoid valve was controlled by a custom-developed graphic user interface (Matlab) (Gomez-Sjoberg et al., 2010), which can also execute pre-written code. Cell chambers were coated with fibronectin (Sigma-Aldrich, FC010), and washed with fresh medium before loading cells. Fibroblasts were loaded at ~70% confluency to collect sufficient single cell data while avoiding significant overlap between cells. After fibroblasts were attached on the substrate, macrophages were loaded at different densities and locations of the chamber as required in the experiment. After waiting 4–6 h to give cells sufficient time to spread out evenly in the chamber, cells were stained with 1 μM Hoescht 33342 if necessary for nucleus tracking, then either TNF-α (R&D Systems, aa80-235) or LPS (InvivoGen, tlrl-3pelps) was loaded in pre-chamber. The formation of the stimulus gradient over the cell population was initiated by opening the separating valve between pre-chamber and cell chamber and by continuously flushing the sink channel at the end of chamber through gentle peristaltic pumping. More details for the experimental setup and procedure are described in the supplemental information.

2.5. Imaging and image analysis

Epifluorescence images were acquired using Nikon Ti2 microscope, and analyzed through custom software. Briefly, our method evaluates the median nucleus and cytosol p65 levels for each cell, and uses the ratio of nucleus over cytosol intensity to quantify activation strength, similar to the method described in previous NF-κB study (Kudo et al., 2018). More details of imaging settings and analysis steps are described in the supplemental information.

2.6. Cell retrieval

Before retrieval, a portion of the chip outlet was cut through the green dotted line (Fig. S1F) and removed. This allowed the retrieved cells to accumulate in a droplet on the glass slide (Fig. 2D), which makes it easier to recover with a pipette. After the desired stimulation interval, TrypLE (Gibco) was flowed through the inlet channel and into the receiving chamber for ~10 s. Before cells detached from the surface, all the valves including the partitioning valves (Fig. 2A) were closed, dividing the chamber into near, mid, and far regions relative to the pre-chamber. Cells in the chamber were further incubated for ~60 s to allow cells to fully detach from the surface, then PBS (Gibco) was rapidly flowed through the cell retrieval channels and to one of the outlets (Fig. S1F, also see Video V1). The vast majority of the cells (~100 per section) come from the corresponding region, with only a few boundary cells being included from the bordering regions. The cells were collected in a ~2 μl droplet, which was then deposited in 10 μL ice cold lysis buffer containing 0.1% Triton-X-100 and RNAse inhibitor (Takara). After retrieving cells from each section of chamber, the channels were flushed with PBS for a few seconds, then the process was repeated to retrieve other samples. Cell retrieval was constantly monitored in real time through microscope. We have tracked more than 100 retrievals without observing signs of significant cross-contamination. After retrieval, the PCR tubes containing cell lysate were stored at −80°C until further processing.

Supplementary video related to this article can be found at https://doi.org/10.1016/j.bios.2023.115089

2.7. qPCR analysis and simulation for downstream gene expression

The retrieved cells were reverse transcribed and pre-amplified according to the SmartSeq2 RNA processing pipeline (Picelli et al., 2014), then the gene expression levels were quantified through qPCR.

Additionally, to compare the NF-κB activity with the downstream gene expression, the expressed mRNA levels were simulated using NF-κB translocation dynamics at each distance as an input to a gene expression equation. More details about the qPCR procedure, primer sequences, and description for fitted parameters and differential equation, can be found in supplemental information.

3. Results and discussions

3.1. Design principle of the high throughput microfluidic co-culture system

We designed a device which allowed us to study two modes of signaling in cell populations: activation of a small group of signaling

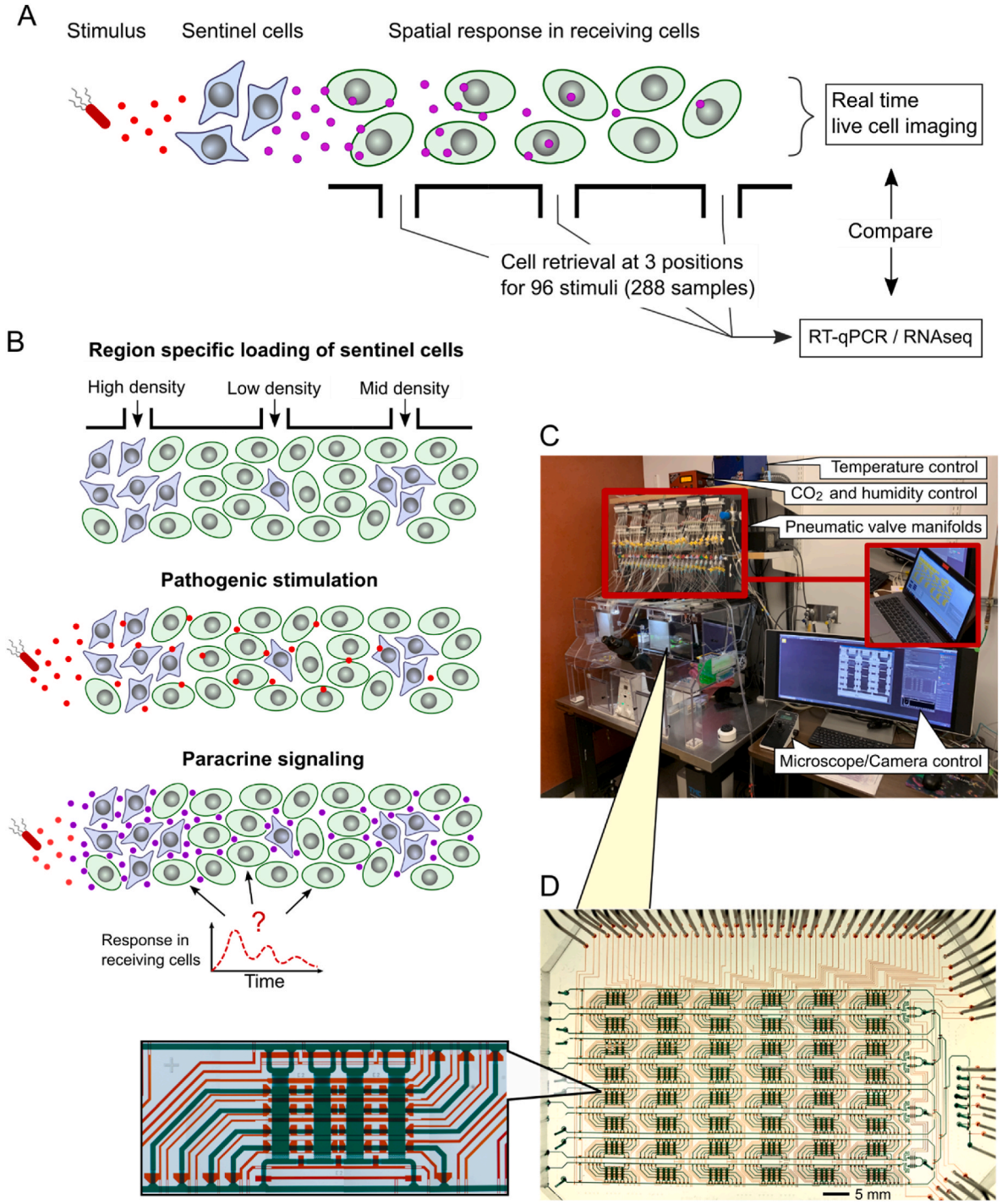

Fig. 1. Overview of the microfluidic co-culture system for testing diverse signaling conditions. (A) The co-culture system enables stimulation of sentinel or signaling cells (blue) located in the pre-chamber. Secreted signals (purple) diffuse into another chamber loaded with receiving cells (green). At three different distances from the pre-chamber, receiving cells can be retrieved and analyzed. (B) The same design can be used to load signaling cells at different concentrations and distributions in a population of receiving cells, modeling the uneven distribution of sentinel cells *in vivo*. (C) Photo of the integrated imaging and chip control apparatus. The microfluidic chip is controlled by a custom GUI and the experiment is automated by custom code (red box). (D) Photo of the two-layer high-throughput co-culture device described in (A) and (B). Red dye fills control channels, while green dye fills the cell chambers and fluid passages. The inset on the left shows one of the repeating units in the design (See Fig. 2A).

cells which communicate with receiving cells (Fig. 1A), and communication among a population with spatially varying densities of signaling and receiving cells (Fig. 1B). Additionally, our device enables live cell imaging of single cells during stimulation and endpoint retrieval of cells based on region for analysis (Fig. 1A). This design is versatile and useful for tracking cellular responses under biologically relevant signaling gradients.

In order to increase precision, we automated control of the device using a custom-developed graphic user interface (GUI) and integrated it with the live cell imaging setup (Fig. 1C). The PDMS-based two-layer microfluidic device is controlled by pneumatic valves, which can be actuated manually or automatically through execution of pre-written scripts. The device is housed in a temperature, CO_2, and humidity controlled live-imaging setup mounted on an epifluorescence microscope (Fig. 1C).

For increased throughput, we incorporated 192 chambers organized in an 8x24 array and multiplexed the control valves for inlet channels (Fig. 1D and Fig. S1). Each of 96 pairs of repeating units can be independently controlled by selecting the desired row and column. In each unit, the smaller pre-chamber and larger receiving chamber are separated by a valve and can be independently loaded with different cell types. The receiving chamber can be partitioned into three regions based on proximity to the pre-chamber. Cells in each region can be retrieved independently through a dedicated side channel (Fig. 1A). Different cell types and densities can also be patterned in each region through these side channels (Fig. 1B). A forest of pillars is placed between the bottom of the receiving chamber and the sink channel. Each sink channel is flushed slowly using peristaltic pumps to provide shear-free sinking of multiple chambers (Fig. 2A and Fig. S1). This sink channel mimics the biological action of capillaries, which provide tissues with nutrients and oxygen and remove waste products and secreted cytokines (Kumar et al., 2019).

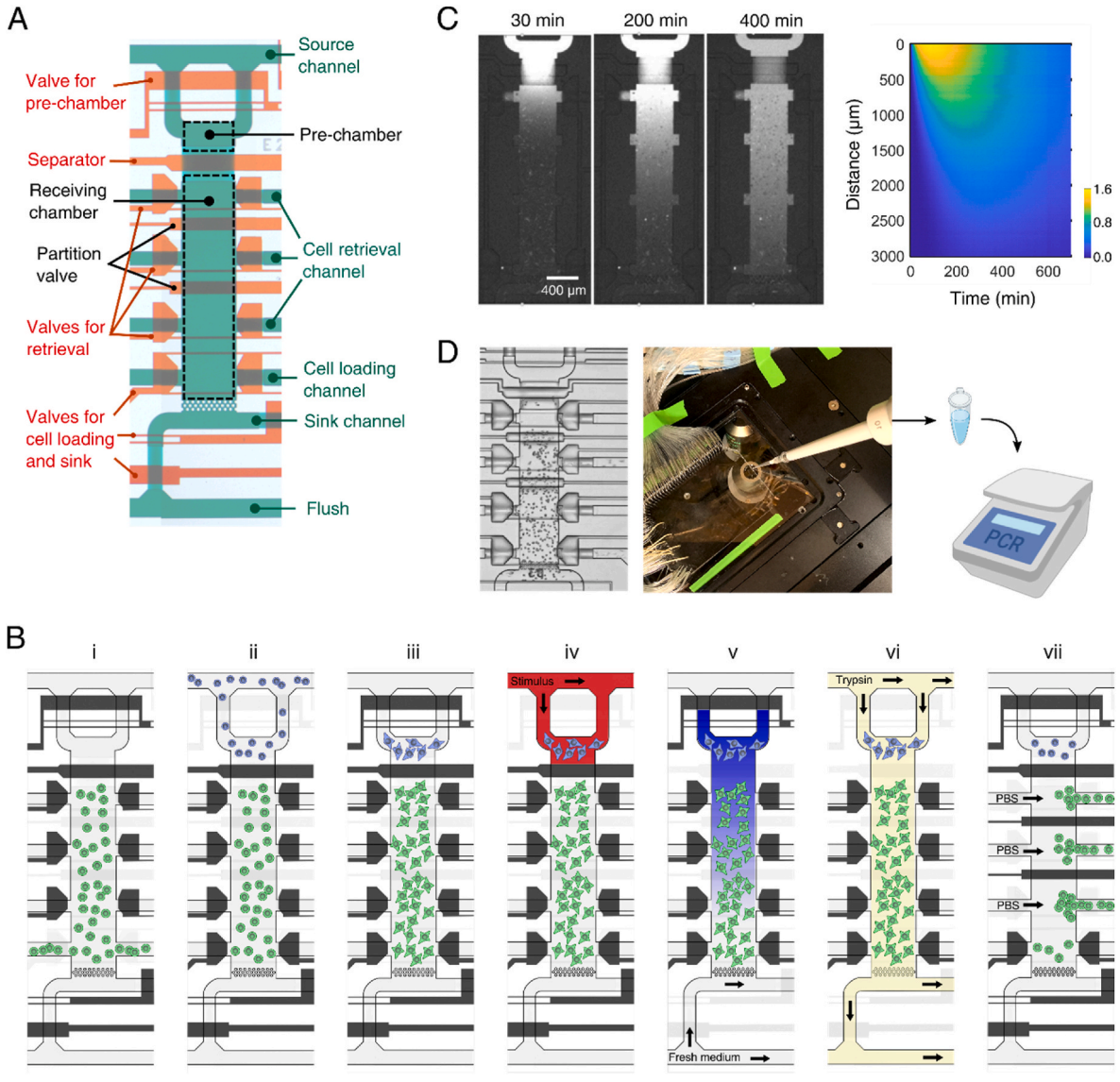

Fig. 2. Co-culture chamber design and procedures for spatially resolved cell-cell communication and cell retrieval. (A) Magnified image of single co-culture unit. Green dye shows the channel and chambers in the fluid layer, while red shows the valves in the control layer. (B) Series of diagrams describe the experimental procedure for pre-chamber stimulation, signal diffusion, and cell retrieval for downstream expression measurement. (C) Demonstration of gradient formation using Cy5. After opening the separator valve, the bottom end of the receiving chamber was continuously washed. Label above each fluorescence image indicates the elapsed time after opening the separator. Heatmap on right shows the kinetics of gradient formation and degradation over the cell chamber. (D) Cells from different positions are trypsinized and flowed to a designated output. The droplet containing cells are retrieved, added into lysis buffer, and processed for measurement of gene expression.

In order to test the control and generation of a diffusion gradient over the receiving chamber, we loaded the pre-chamber with cyanine 5 (Cy5) and opened the separator while flushing the sink channel (Fig. 2C). We observed a rapid increase in fluorescence in the receiving chamber near the pre-chamber, followed by a gradual increase in fluorescence in farther regions of the receiving chamber. Our chip successfully "grounded" the fluorescence at the bottom of the chamber near zero without disturbing the gradient across the chamber (Fig. 2C).

3.2. Operation of the co-culture device for the study of cell-cell signaling and cell retrieval

To study the signaling processes involved in sentinel cell detection of pathogens and communication with neighboring cells, we used a lipopolysaccharide (LPS)-macrophage-fibroblast model (Fig. 1A). LPS is a potent activator of inflammatory signaling in sentinel macrophages (Lu et al., 2008). These macrophages then secrete numerous proinflammatory cytokines, which act on fibroblasts and other tissue cells in the local environment to relay the inflammatory response (Frank and Tay, 2015; Junkin et al., 2016; Neupane et al., 2020; Sheu et al., 2019; Son et al., 2022).

We tracked activation and propagation of signaling in this system through measuring NF-κB activation dynamics, which play a central role in inflammatory signaling (Hoffmann et al., 2002; Junkin et al., 2016; Kellogg et al., 2015; Son et al., 2022; Tay et al., 2010). We loaded RelA-DsRed tagged RelA$^{-/-}$ 3T3 fibroblasts (3T3s) through the cell loading channel into the receiving chamber (Fig. 2B i) (DeFelice et al., 2019). Then, RAW264.7 macrophage-like cells expressing RelA-GFP were loaded into the pre-chamber through the source channel (Fig. 2B ii) (Junkin et al., 2016). We tracked activation of the canonical NF-κB pathway by monitoring nuclear translocation of RelA. We exposed the macrophages to 50 ng/mL of LPS (Fig. 2B iii — iv) for 10 min, then washed them with fresh medium to remove the LPS. We then opened the separator valve to allow secreted cytokines to diffuse into the receiving chamber (Fig. 2B v). For downstream gene expression measurements, each pair of chambers was filled with trypsin to begin detaching cells (Fig. 2B vi), then the partitioning valves were closed. Detached cells in each region were flowed out, collected from the outlet (Fig. S1F), and placed into lysis buffer (Fig. 2B vii, D, also see Video V1). The lysates can be stored long-term at −80°C and are suitable for qPCR or RNA sequencing. This approach combines isolated stimulation of a subpopulation of cells, generation of a signaling gradient, live cell imaging, and region-based gene expression measurement. These features present a significant advance over other methods for spatially resolved study of cell-cell communication and signaling.

3.3. High throughput testing of co-culture conditions reveals correlation between signaling range and macrophage densities, and heterogeneity in responding populations

Using this approach, we tracked signaling between 10 and 100 LPS-stimulated RAW macrophages and a large population of 3T3s (200 — 400 cells). We visualized fibroblast responses throughout the receiving chamber as macrophage-secreted cytokines diffused through the chamber (Fig. 3A and B; Fig. S2 and S3 for examples of single cell traces and macrophage images; also see Video V2). We noticed significant changes in the signaling range (distance to farthest activated fibroblast) depending on the macrophage number, with more macrophages in the pre-chamber exhibiting NF-κB activation at longer distances (Fig. 3B). However, samples with similar macrophage numbers produced comparable signaling ranges (Fig. 3C). These results suggest that signaling range is determined by sentinel macrophage number despite heterogeneity within macrophage and fibroblast populations. Previously, we showed that while fibroblast variability does not affect signaling range or mean NF-κB behavior at various distances, single macrophage variability can significantly change both (Son et al., 2022). In this work, however, we observed that at increased macrophage densities, macrophage variability is buffered and signaling range becomes consistent. Nonetheless, heterogeneity within the macrophage population can still play a major role in determining fibroblast dynamics. Even between conditions with similar, large numbers of macrophages (~60), fibroblast response dynamics varied widely, especially during the later period of activation (Fig. 3C). Response heterogeneity in sentinel cells is well established, and early responding sentinel cells play a crucial role in

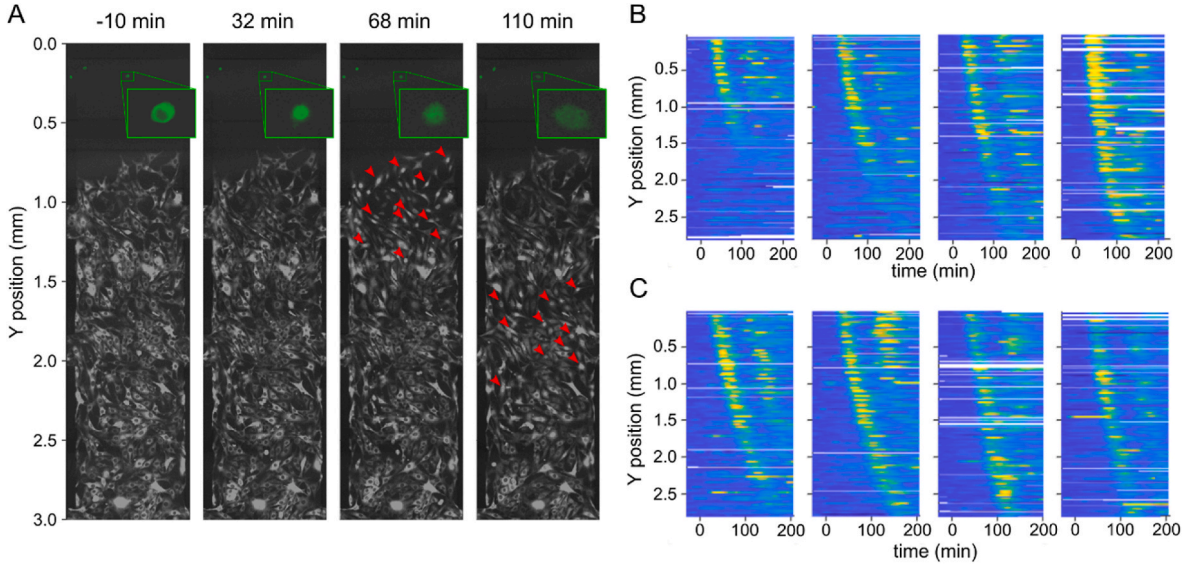

Fig. 3. Macrophage to fibroblast signaling experiments reveal how heterogeneity in the signaling population produces variable responses in the receiving population. (A) Fluorescence images show stimulated RAWs (green) secreting products which activate the 3T3 population over space (black and white). At −10 min, the pre-chamber was filled with medium containing 50 ng/ml LPS. At 0 min, the pre-chamber was washed with fresh medium and the separator was opened. The inset in the green box shows the example of NF-κB activation in a RAW cell, while the red arrows indicate the examples of activated 3T3s. (B) Heatmap showing single fibroblast NF-κB dynamics by distance from the macrophages. Different number of macrophages (roughly 10, 30, 60, and 100 macrophages from left to right) were loaded in the pre-chamber and were stimulated with 50 ng/ml LPS for 10 min. (C) Same as (B) but from samples with similar number of macrophages (~60) to show variability in activation dynamics.

paracrine signaling and development of initial immune response in larger populations (Alexander et al., 2021; Avraham et al., 2015; Junkin et al., 2016; Kaestli et al., 2017; Lee et al., 2009; Shalek et al., 2014; Xue et al., 2015). Here, we demonstrate that heterogeneity in a population of sentinel macrophage does not affect the signaling range but still significantly influences response dynamics in tissue-like mixed cell populations.

Supplementary video related to this article can be found at https://doi.org/10.1016/j.bios.2023.115089

3.4. Co-culture system enables spatially resolved gene expression measurements downstream of NF-κB

To demonstrate the ability of our system to measure gene expression based on distance to a signaling source, we first used a simplified model of cellular communication. Previous studies showed that TNF-α is the dominant NF-κB-activating ligand released during the early inflammatory period; however its secretion level can vary significantly between macrophages (Adelaja et al., 2021; Junkin et al., 2016; Son et al., 2022). Thus, for consistent and accurate comparison between multiple samples, 30 ng/ml of TNF-α was loaded into the pre-chamber and the separator was opened to simulate the early phase of an inflammatory stimulus. 3T3s near the pre-chamber displayed rapid and strong NF-κB activation dynamics, followed by rapid decrease in activation (Fig. 4A). In contrast, 3T3s in farther regions activated more slowly and with lower activation amplitudes. Additionally, the activation dynamics became more heterogeneous at farther regions, with variable activation times and oscillatory periods, possibly due to lower concentration of TNF in this region (Tay et al., 2010). These results largely reproduced results from the co-culture experiments (Fig. 3).

To evaluate the high-throughput capability of our system in examining gene expressions from specific regions, we measured the kinetics of gene expression in all three positions after TNF-α stimulation. For all positions, cells were collected in triplicate at 0, 1, 2, 4, 6, and 8 h after opening the separator. The collected cells were lysed and kept on ice. After reverse-transcription and pre-amplification (Kellogg et al., 2014; Son et al., 2021), we quantified three well-studied NF-κB response genes (*Tnfaip3*, *Casp4*, and *Ccl5*) and a control gene (*GAPDH*) using qPCR (Son et al., 2022; Tay et al., 2010). *Tnfaip3* (A20) is strongly induced and rapidly degraded during constant stimulation with TNF-α (Tay et al., 2010), while *Ccl5* (RANTES) and *Casp4* (CASP4) accrue gradually during constant stimulation (Tay et al., 2010). By measuring these genes, we studied how different expression profiles of NF-κB target genes affect their response at different distance from the signal-secreting source. In near positions, *Tnfaip3* rose rapidly after exposure to TNF-α, peaking at 60 min after opening of the separator and decreasing rapidly (Fig. 4B). However, in mid and far positions, *Tnfaip3* rose more gradually and to a lesser extent, peaking at 120 min after opening of the separator. Thus, the transcriptional dynamics of *Tnfaip3* are sensitive to distance and regional cytokine profile. In contrast, *Ccl5* and *Casp4* rose gradually over time in all positions, peaking at 4 — 6 h after opening of the separator and decreasing slowly (Fig. 4B). The magnitude of increase was also

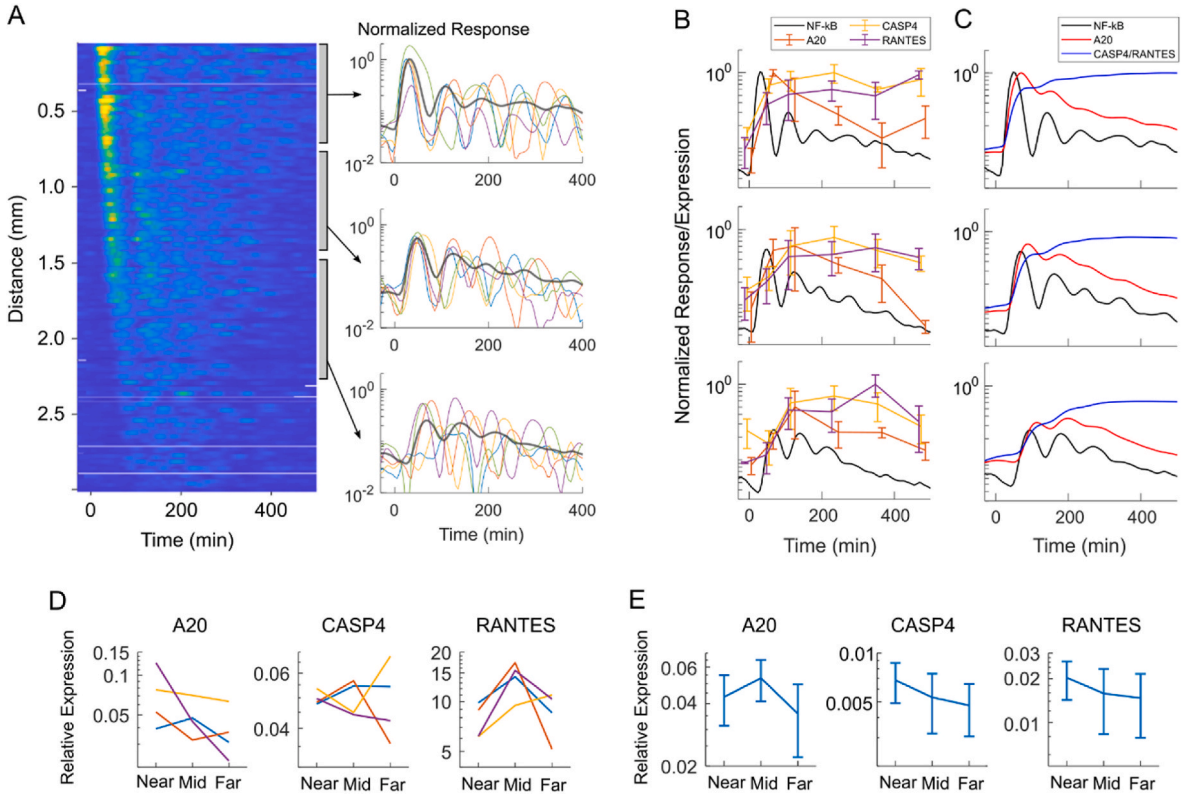

Fig. 4. Spatiotemporal gene expression measurements show different spatial expression dynamics. (A) 30 ng/ml of TNF-α was loaded in the pre-chamber and allowed to diffuse into the receiving chamber loaded with 3T3s. The heatmap shows the dynamics of single cell NF-κB dynamics (>600 cells) at various distances from pre-chamber. Thin colored lines on the right show six random single cell traces from three different regions, while thick black lines show the median behavior in corresponding region. (B) Median NF-κB dynamics were tracked from each region (black lines) and overlaid with gene expression from three NF-κB target genes (A20, CASP4, and RANTES). The error bar indicates the standard deviation from three biological replicates. Each gene level is normalized to the maximum level measured in all samples. (C) Using median NF-κB dynamics as an input, downstream gene expression is simulated through an ordinary differential equation. Red indicates early genes with fast degradation rate, while blue indicates late genes with slow degradation rate. (D) Spatial gene expression measurements were performed using similar number of macrophages (60 ± 15) instead of fixed dose of TNF-α. At 4 h, cells from three different regions were retrieved and their gene expressions were quantified. Four colored lines indicate the expression levels from four different samples. (E) For easy comparison, the gene expression levels at 4 h from previous 30 ng/ml TNF-α is replotted in the same format.

similar for all three positions. Thus, late genes appear to be less sensitive to distance in their transcriptional dynamics.

Degradation rate plays a key role in determining dynamics of NF-κB target gene expression (Sen et al., 2020; Tay et al., 2010); which led us to hypothesize it also plays a significant role in each gene's sensitivity to distance. To briefly examine this hypothesis, we simulated the kinetics of target gene expression with various degradation rates. We used the measured NF-κB dynamics (black lines in Fig. 4B and C) as an input to a simple gene expression equation, and changed the degradation rate by 20-fold while keeping other parameters similar to each other (less than 0.3-fold difference, Methods) (Alon, 2006). Our simulation with just one differential equation successfully reproduced complex gene expression profiles occurring at different distances from source (Fig. 4C), which suggests that the different degradation rate can explain distance-dependent patterns of gene expression.

Although inducing reproducible NF-κB activation profiles across samples was not feasible with macrophages due to cellular variability (Fig. 3C), we still tried to measure regional gene expression from individual chambers in our co-culture setup. Instead of a fixed concentration of TNF-α, we loaded macrophages (60 ± 15) in the pre-chamber, stimulated with 50 ng/ml LPS for 10 min, washed with fresh medium, and opened the separator to initiate signaling between the two populations. After 4 h, cells from three different regions were retrieved and their gene expression levels quantified. In these experiments, gene expression

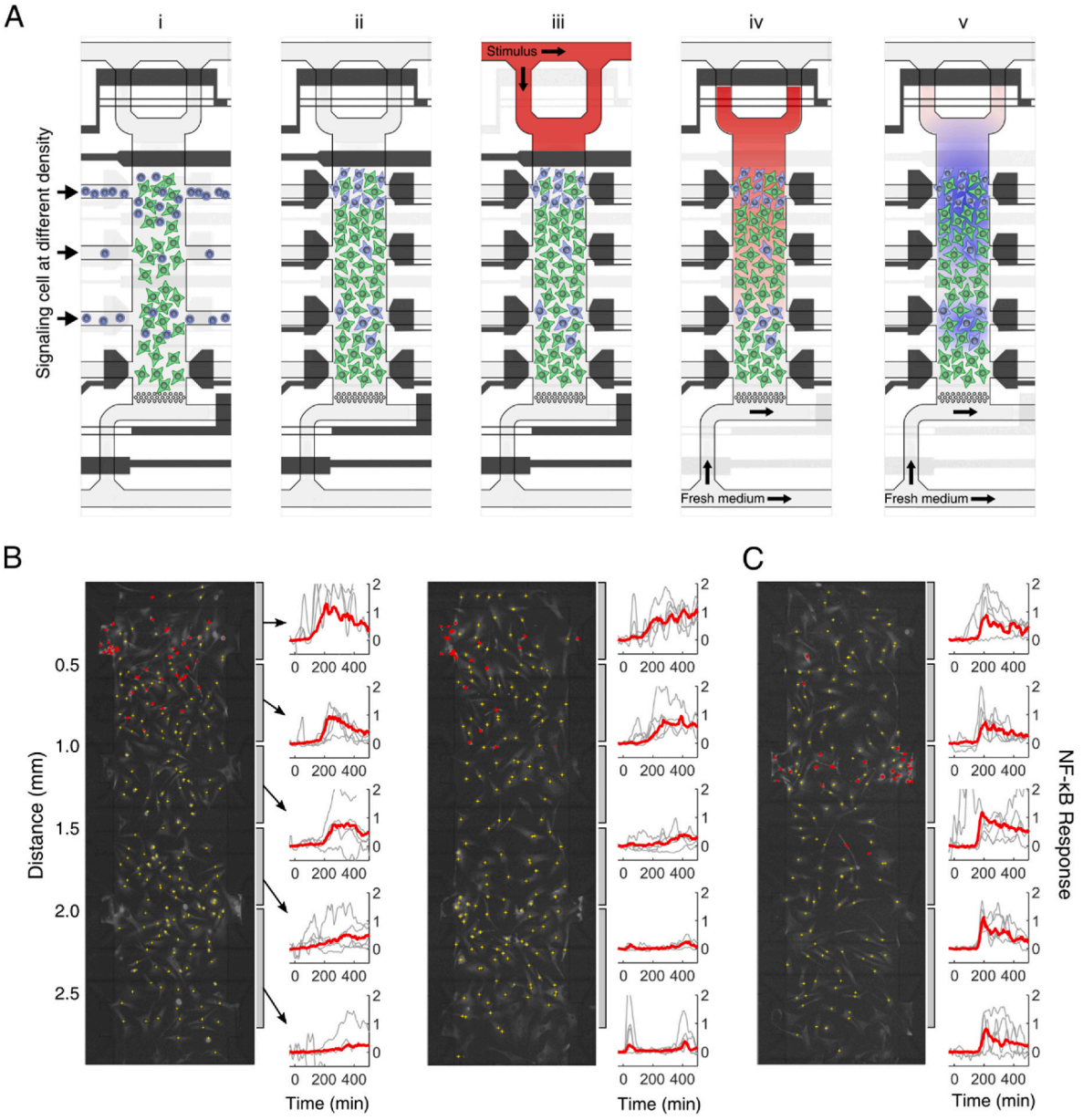

Fig. 5. Spatially-patterned co-culture experiments show how distribution of sentinel cells affects the response in population level. (A) Diagrams illustrate the procedures for patterning cell distributions in our device: i) different densities of macrophages are loaded in each region of the cell chamber, ii) cells are allowed to adapt to the device, iii) stimulus is loaded in the pre-chamber, iv) stimulus diffusion is initiated, and v) secretion from macrophages activate other cells. (B) Primary fibroblasts are loaded throughout the cell chamber (yellow crosses), then bone-marrow-derived macrophages (red circles) are loaded close to the pre-chamber at two different densities. After releasing 3 ng/ml LPS from pre-chamber, NF-κB dynamics in fibroblasts are evaluated and plotted on the right. Gray lines show five random single cell dynamics, while red lines show the median dynamics in each region (Fig. S4 for more detailed single cell traces). (C) Macrophages are loaded in the middle of the cell chamber through different side channels, and resulting NF-κB dynamics in fibroblasts are plotted on the right similar to (B) (Fig. S5 for more detailed single cell traces).

patterns varied from the fixed dose experiments (Fig. 4D and E). For example, A20 showed the highest expression at early positions in contrast to mid positions from fixed TNF-α dose experiments, while Ccl5 (RANTES) showed the highest expression levels at mid positions. These differences could be due to different TNF-α secretion profile from macrophages and/or other cytokines secreted by macrophages.

3.5. Spatial distribution and density of sentinel cells determines local NF-κB response

Our new design also allows different cell types and densities to be patterned throughout the receiving chamber (Fig. 2A). For example, fibroblasts can be loaded throughout the chamber (Fig. 5A i) and different macrophage densities can be patterned through the side channels (Fig. 5 ii). By varying the density of macrophages in each region, our chip can reproduce an arbitrary combination of macrophage-fibroblast densities. Thus, our chip can simulate an infection scenario in which cell populations with different distributions of sentinel cells densities are exposed to a bacterial challenge (Fig. 5A iii-iv).

First, to demonstrate our device's ability to control regional cell density, we prepared two different concentrations of macrophages and loaded them in the near position of two different chambers pre-loaded with fibroblasts (Fig. 5B). To increase the relevance of our study to *in vivo* inflammatory signaling, we used primary murine adult fibroblasts and bone-marrow-derived-macrophages from a mouse expressing endogenously tagged RelA-YFP for this test (Adelaja et al., 2021). After loading cells, we filled the pre-chamber with a low dose of LPS (3 ng/mL) and opened the separating valve to expose the macrophage-fibroblast co-culture to diffusing pathogenic signals and secreted molecules. This LPS dose is low enough that fibroblasts do not respond (Kellogg et al., 2015). Thus, any NF-κB activation in fibroblasts would be due to LPS-induced secretion by the macrophages. When a different density of macrophages was loaded in the same position in fibroblast population, we observed a dramatic change in the signaling range (Fig. 5B). The lower macrophage number in the early position resulted in a shorter signaling range, which also corresponds with our results from the pre-chamber experiments (Fig. 3B).

To further demonstrate the cell patterning capability of our device, we loaded macrophages at two different locations in the cell chamber and initiated the inflammatory signaling with the same dose of LPS (3 ng/ml) (Fig. 5B and C). We observed that when macrophages were loaded near the signaling source (0–0.5 mm away), neighboring fibroblasts exhibited strong NF-κB activation, while fibroblasts farther from the macrophages and LPS source responded weakly, and in a delayed manner over the course of imaging (Fig. 5B and S4). Similarly, when macrophages were loaded in the middle of cell chamber (1–1.5 mm away from the signaling source), fibroblast activation is strongest and most rapid in cells neighboring the macrophages (Fig. 5C, S5, also see Video V3). However, this fibroblast activation was weaker than when macrophages were loaded close to the LPS source. This observation could be explained by the longer distance between macrophages and the LPS source producing reduced cytokine secretion by macrophages. Most fibroblasts throughout the chamber displayed an obvious response when macrophages were loaded in the middle of the chamber, in contrast to the weak response or lack of response in the farthest positions when macrophages were loaded close to the source (Fig. 5C and S5). These results indicate that the spatial distribution of sentinel cells in a population can significantly affect population level response to a pathogenic stimulus.

Supplementary video related to this article can be found at https://doi.org/10.1016/j.bios.2023.115089

4. Conclusion

Previous theoretical and experimental studies highlighted how distance and distribution of specialized cells shape the course of biological phenomena in developmental biology (Christian, 2012; Zinski et al., 2017), chemotaxis (Ambravaneswaran et al., 2010), and immunology (Oyler-Yaniv et al., 2017). Particularly in the context of infection and inflammation, sentinel cells play a vital role in interpreting external signals and coordinating population-level responses through paracrine signaling (Alexander et al., 2021; Lee et al., 2009; Neupane et al., 2020; Oyler-Yaniv et al., 2021; Shalek et al., 2014). Up to this point, however, it has been difficult to reproduce and model the cell-cell interactions, which take place in a spatially resolved and physiological manner. Many attempts to understand spatial signaling relationships are inferred from staining fixed tissue (Christian, 2012; Oyler-Yaniv et al., 2017) or deconvolution of single-cell transcriptomic data (Cang and Nie, 2020; Jin et al., 2021). Furthermore, attempts to experimentally model spatial diffusion of signaling molecules are often limited by low throughput of custom systems (Ambravaneswaran et al., 2010; Frank and Tay, 2015) or reliance on semi-solid medium which restricts cell movement (Dilanji et al., 2012; Ellison et al., 2016).

In this study, we present a new microfluidic design and protocol for generating and testing signal gradients and manipulate cell distributions in unprecedented scale. Through high-level of multiplexing and parallel peristaltic pumping, our new device enables independent stimulation of subpopulations of cells, formation of a signal gradient over the cell population, spatially resolved cell retrieval for gene expression analysis, and control of the cell densities and types at specific locations, all at high-throughput. Furthermore, we automate the operation of the device to precisely and consistently execute experiments, and integrated epi-fluorescence microscopy to track single cell behavior. Our brief tests to demonstrate these functions resulted in multiple unprecedented findings addressing the role of signal diffusion and impact of heterogeneous cell population in innate immune signaling (Fig. 3—5). Our design therefore addresses key challenges in studying spatial and temporal aspects of cell-cell signaling.

However, our design has limitations, particularly with measurement or control at the single cell level. For instance, cell retrieval is only possible from three regions of the receiving chambers. Modifying the device or employing additional cell marking methods such as photo-activatable dyes may increase spatial resolution, while integrating single cell sequencing techniques could allow single cell resolution (Genshaft et al., 2021). Additionally, over the course of testing, we found accurate control over cell densities can be challenging especially at the single cell level. Due to large dead volumes in fluid channels and relatively slow response time of valves due to length of control channels, trapping single cells in the pre-chamber turned out to be difficult. Either optimizing fluid channels for single cell loading, possibly with single cell traps, or decreasing valve response time by shortening control line lengths (at the cost of lower throughput) can improve this.

Although our tests mainly focused on innate immune signaling, we highlight that our device is broadly applicable to modeling signal diffusion and evaluating transcriptomic effects in other contexts. For example, morphogenic and chemotactic gradients play important roles in embryo development and in immune cell recruitment, respectively. While a number of computational models have been proposed to explain these phenomena (Durrieu et al., 2018; Ellison et al., 2016; Mugler et al., 2016; Zinski et al., 2017), our device enables direct testing of those complex and biologically important models.

CRediT authorship contribution statement

Minjun Son: Conceptualization, Methodology, Software, Validation, Formal analysis, Investigation, Data curation, Writing – original draft, Writing – review & editing, Visualization, Supervision, Project administration. **Andrew G. Wang:** Validation, Formal analysis, Investigation, Writing – original draft, Writing – review & editing, Visualization. **Emma Kenna:** Investigation, Writing – original draft. **Savaş Tay:** Resources, Data curation, Writing – original draft, Writing – review & editing, Supervision, Project administration, Funding acquisition.

Declaration of competing interest

The authors declare that they have no known competing financial interests or personal relationships that could have appeared to influence the work reported in this paper.

Data availability

Single cell data and codes for figures have been deposited in Github (https://github.com/tay-lab/High-throughput-co-culture-system).

Acknowledgements

This work is supported by NIH Grants R01GM128042 and R01GM127527 (S.T.). M.S. is supported by the ImEPosT training grant NIAID 5T32AI153020. A.G.W. is supported by the NIH MSTP training grant T32GM07281. qPCR was performed at the Single Cell Immunophenotyping Core of the University of Chicago. Authors want to thank Dr. Jing Lin for her help with mold fabrication, Dr. Bijentimala Keisham and Peer M.S.M. Rahman for their help with discussion and proofreading.

Appendix A. Supplementary data

Supplementary data to this article can be found online at https://doi.org/10.1016/j.bios.2023.115089.

References

Adelaja, A., Taylor, B., Sheu, K.M., Liu, Y., Luecke, S., Hoffmann, A., 2021. Six distinct NFκB signaling codons convey discrete information to distinguish stimuli and enable appropriate macrophage responses. Immunity 54, 916–930.e7. https://doi.org/10.1016/j.immuni.2021.04.011.

Alexander, A.F., Kelsey, I., Forbes, H., Miller-Jensen, K., 2021. Single-cell secretion analysis reveals a dual role for IL-10 in restraining and resolving the TLR4-induced inflammatory response. Cell Rep. 36, 109728 https://doi.org/10.1016/j.celrep.2021.109728.

Alon, U., 2006. An Introduction to Systems Biology: Design Principles of Biological Circuits. CRC Press.

Ambravaneswaran, V., Wong, I.Y., Aranyosi, A.J., Toner, M., Irimia, D., 2010. Directional decisions during neutrophil chemotaxis inside bifurcating channels. Integr Biol (Camb) 2, 639–647. https://doi.org/10.1039/c0ib00011f.

Avraham, R., Haseley, N., Brown, D., Penaranda, C., Jijon, H.B., Trombetta, J.J., Satija, R., Shalek, A.K., Xavier, R.J., Regev, A., Hung, D.T., 2015. Pathogen cell-to-cell variability drives heterogeneity in host immune responses. Cell 162, 1309–1321. https://doi.org/10.1016/j.cell.2015.08.027.

Cang, Z., Nie, Q., 2020. Inferring spatial and signaling relationships between cells from single cell transcriptomic data. Nat. Commun. 11, 2084. https://doi.org/10.1038/s41467-020-15968-5.

Chang, C.-W., Cheng, Y.-J., Tu, M., Chen, Y.-H., Peng, C.-C., Liao, W.-H., Tung, Y.-C., 2014. A polydimethylsiloxane–polycarbonate hybrid microfluidic device capable of generating perpendicular chemical and oxygen gradients for cell culture studies. Lab Chip 14, 3762–3772. https://doi.org/10.1039/C4LC00732H.

Christian, J.L., 2012. Morphogen Gradients in Development: from Form to Function, 1. Wiley Interdiscip Rev Dev Biol, pp. 3–15. https://doi.org/10.1002/wdev.2.

Daniels, R., Vanderleyden, J., Michiels, J., 2004. Quorum sensing and swarming migration in bacteria. FEMS (Fed. Eur. Microbiol. Soc.) Microbiol. Rev. 28, 261–289. https://doi.org/10.1016/j.femsre.2003.09.004.

DeFelice, M.M., Clark, H.R., Hughey, J.J., Maayan, I., Kudo, T., Gutschow, M.V., Covert, M.W., Regot, S., 2019. NF-B signaling dynamics is controlled by a dose-sensing autoregulatory loop. Sci. Signal. 12, eaau3568. https://doi.org/10.1126/scisignal.aau3568.

Dilanji, G.E., Langebrake, J.B., De Leenheer, P., Hagen, S.J., 2012. Quorum activation at a distance: spatiotemporal patterns of gene regulation from diffusion of an autoinducer signal. J. Am. Chem. Soc. 134, 5618–5626. https://doi.org/10.1021/ja211593q.

Durrieu, L., Kirrmaier, D., Schneidt, T., Kats, I., Raghavan, S., Hufnagel, L., Saunders, T. E., Knop, M., 2018. Bicoid gradient formation mechanism and dynamics revealed by protein lifetime analysis. Mol. Syst. Biol. 14, e8355 https://doi.org/10.15252/msb.20188355.

Ellison, D., Mugler, A., Brennan, M.D., Lee, S.H., Huebner, R.J., Shamir, E.R., Woo, L.A., Kim, J., Amar, P., Nemenman, I., Ewald, A.J., Levchenko, A., 2016. Cell–cell communication enhances the capacity of cell ensembles to sense shallow gradients during morphogenesis. Proc. Natl. Acad. Sci. USA 113, E679–E688. https://doi.org/10.1073/pnas.1516503113.

Englert, D.L., Manson, M.D., Jayaraman, A., 2009. Flow-based microfluidic device for quantifying bacterial chemotaxis in stable, competing gradients. Appl. Environ. Microbiol. 75, 4557–4564. https://doi.org/10.1128/AEM.02952-08.

Frank, T., Tay, S., 2015. Automated co-culture system for spatiotemporal analysis of cell-to-cell communication. Lab Chip 15, 2192–2200. https://doi.org/10.1039/c5lc00182j.

Genshaft, A.S., Ziegler, C.G.K., Tzouanas, C.N., Mead, B.E., Jaeger, A.M., Navia, A.W., King, R.P., Mana, M.D., Huang, S., Mitsialis, V., Snapper, S.B., Yilmaz, Ö.H., Jacks, T., Van Humbeck, J.F., Shalek, A.K., 2021. Live cell tagging tracking and isolation for spatial transcriptomics using photoactivatable cell dyes. Nat. Commun. 12, 4995. https://doi.org/10.1038/s41467-021-25279-y.

Gomez-Sjoberg, R., Leyrat, A.A., Houseman, B.T., Shokat, K., Quake, S.R., 2010. Biocompatibility and reduced drug absorption of Sol−Gel-treated poly(dimethyl siloxane) for microfluidic cell culture applications. Anal. Chem. 82, 8954–8960. https://doi.org/10.1021/ac101870s.

Handly, L.N., Pilko, A., Wollman, R., 2015. Paracrine communication maximizes cellular response fidelity in wound signaling. Elife 4, e09652. https://doi.org/10.7554/eLife.09652.

Handly, L.N., Wollman, R., 2017. Wound-induced Ca2+ wave propagates through a simple release and diffusion mechanism. MBoC 28, 1457–1466. https://doi.org/10.1091/mbc.e16-10-0695.

Hind, L.E., Ingram, P.N., Beebe, D.J., Huttenlocher, A., 2018. Interaction with an endothelial lumen increases neutrophil lifetime and motility in response to P aeruginosa. Blood 132, 1818–1828. https://doi.org/10.1182/blood-2018-05-848465.

Hoffmann, A., Levchenko, A., Scott, M.L., Baltimore, D., 2002. The IκB-NF-κB signaling module: temporal control and selective gene activation. Science 298, 1241–1245. https://doi.org/10.1126/science.1071914.

Jin, S., Guerrero-Juarez, C.F., Zhang, L., Chang, I., Ramos, R., Kuan, C.-H., Myung, P., Plikus, M.V., Nie, Q., 2021. Inference and analysis of cell-cell communication using CellChat. Nat. Commun. 12, 1088. https://doi.org/10.1038/s41467-021-21246-9.

Josan, S., Spielman, D., Yen, Y.-F., Hurd, R., Pfefferbaum, A., Mayer, D., 2012. Fast volumetric imaging of ethanol metabolism in rat liver with hyperpolarized [1-(13) C]pyruvate. NMR Biomed. 25, 993–999. https://doi.org/10.1002/nbm.2762.

Junkin, M., Kaestli, A.J., Cheng, Z., Jordi, C., Albayrak, C., Hoffmann, A., Tay, S., 2016. High-content quantification of single-cell immune dynamics. Cell Rep. 15, 411–422. https://doi.org/10.1016/j.celrep.2016.03.033.

Kaestli, A.J., Junkin, M., Tay, S., 2017. Integrated platform for cell culture and dynamic quantification of cell secretion. Lab Chip 17, 4124–4133. https://doi.org/10.1039/C7LC00839B.

Kellogg, R.A., Gómez-Sjöberg, R., Leyrat, A.A., Tay, S., 2014. High-throughput microfluidic single-cell analysis pipeline for studies of signaling dynamics. Nat. Protoc. 9, 1713–1726. https://doi.org/10.1038/nprot.2014.120.

Kellogg, R.A., Tian, C., Lipniacki, T., Quake, S.R., Tay, S., 2015. Digital signaling decouples activation probability and population heterogeneity. Elife 4, e08931. https://doi.org/10.7554/eLife.08931.

Kudo, T., Jeknić, S., Macklin, D.N., Akhter, S., Hughey, J.J., Regot, S., Covert, M.W., 2018. Live-cell measurements of kinase activity in single cells using translocation reporters. Nat. Protoc. 13, 155–169. https://doi.org/10.1038/nprot.2017.128.

Kumar, S., Sharife, H., Kreisel, T., Mogilevsky, M., Bar-Lev, L., Grunewald, M., Aizenshtein, E., Karni, R., Paldor, I., Shlomi, T., Keshet, E., 2019. Intra-tumoral metabolic zonation and resultant phenotypic diversification are dictated by blood vessel proximity. Cell Metabol. 30, 201–211.e6. https://doi.org/10.1016/j.cmet.2019.04.003.

Lee, T.K., Denny, E.M., Sanghvi, J.C., Gaston, J.E., Maynard, N.D., Hughey, J.J., Covert, M.W., 2009. A noisy paracrine signal determines the cellular NF-κB response to lipopolysaccharide. Sci. Signal. 2 https://doi.org/10.1126/scisignal.2000599 ra65–ra65.

Lu, Y.-C., Yeh, W.-C., Ohashi, P.S., 2008. LPS/TLR4 signal transduction pathway. Cytokine 42, 145–151. https://doi.org/10.1016/j.cyto.2008.01.006.

Madura, J.D., Briggs, J.M., Wade, R.C., Davis, M.E., Luty, B.A., Ilin, A., Antosiewicz, J., Gilson, M.K., Bagheri, B., Scott, L.R., McCammon, J.A., 1995. Electrostatics and diffusion of molecules in solution: simulations with the University of Houston Brownian Dynamics program. Comput. Phys. Commun. 91, 57–95. https://doi.org/10.1016/0010-4655(95)00043-F.

Mugler, A., Levchenko, A., Nemenman, I., 2016. Limits to the precision of gradient sensing with spatial communication and temporal integration. Proc. Natl. Acad. Sci. USA 113, E689–E695. https://doi.org/10.1073/pnas.1509597112.

Neupane, A.S., Willson, M., Chojnacki, A.K., Vargas E Silva Castanheira, F., Morehouse, C., Carestia, A., Keller, A.E., Peiseler, M., DiGiandomenico, A., Kelly, M. M., Amrein, M., Jenne, C., Thanabalasuriar, A., Kubes, P., 2020. Patrolling alveolar macrophages conceal bacteria from the immune system to maintain homeostasis. Cell 183, 110–125.e11. https://doi.org/10.1016/j.cell.2020.08.020.

Oyler-Yaniv, A., Oyler-Yaniv, J., Whitlock, B.M., Liu, Z., Germain, R.N., Huse, M., Altan-Bonnet, G., Krichevsky, O., 2017. A tunable diffusion-consumption mechanism of cytokine propagation enables plasticity in cell-to-cell communication in the immune system. Immunity 46, 609–620. https://doi.org/10.1016/j.immuni.2017.03.011.

Oyler-Yaniv, J., Oyler-Yaniv, A., Maltz, E., Wollman, R., 2021. TNF controls a speed-accuracy tradeoff in the cell death decision to restrict viral spread. Nat. Commun. 12, 2992. https://doi.org/10.1038/s41467-021-23195-9.

Parsek, M.R., Greenberg, E.P., 2005. Sociomicrobiology: the connections between quorum sensing and biofilms. Trends Microbiol. 13, 27–33. https://doi.org/10.1016/j.tim.2004.11.007.

Picelli, S., Faridani, O.R., Björklund, Å.K., Winberg, G., Sagasser, S., Sandberg, R., 2014. Full-length RNA-seq from single cells using Smart-seq2. Nat. Protoc. 9, 171–181. https://doi.org/10.1038/nprot.2014.006.

Riegman, M., Bradbury, M.S., Overholtzer, M., 2019. Population dynamics in cell death: mechanisms of propagation. Trends Cancer 5, 558–568. https://doi.org/10.1016/j.trecan.2019.07.008.

Selimović, Š., Sim, W.Y., Kim, S.B., Jang, Y.H., Lee, W.G., Khabiry, M., Bae, H., Jambovane, S., Hong, J.W., Khademhosseini, A., 2011. Generating nonlinear concentration gradients in microfluidic devices for cell studies. Anal. Chem. 83, 2020–2028. https://doi.org/10.1021/ac2001737.

Sen, S., Cheng, Z., Sheu, K.M., Chen, Y.H., Hoffmann, A., 2020. Gene regulatory strategies that decode the duration of NFκB dynamics contribute to LPS- versus TNF-specific gene expression. Cell Syst. 10, 169–182.e5. https://doi.org/10.1016/j.cels.2019.12.004.

Shalek, A.K., Satija, R., Shuga, J., Trombetta, J.J., Gennert, D., Lu, D., Chen, P., Gertner, R.S., Gaublomme, J.T., Yosef, N., Schwartz, S., Fowler, B., Weaver, S., Wang, J., Wang, X., Ding, R., Raychowdhury, R., Friedman, N., Hacohen, N., Park, H., May, A.P., Regev, A., 2014. Single cell RNA Seq reveals dynamic paracrine control of cellular variation. Nature 510, 363–369. https://doi.org/10.1038/nature13437.

Sheu, K., Luecke, S., Hoffmann, A., 2019. Stimulus-specificity in the responses of immune sentinel cells. Curr. Opin. Struct. Biol. 18, 53–61. https://doi.org/10.1016/j.coisb.2019.10.011.

Son, M., Frank, T., Holst-Hansen, T., Wang, A.G., Junkin, M., Kashaf, S.S., Trusina, A., Tay, S., 2022. Spatiotemporal NF-κB dynamics encodes the position, amplitude, and duration of local immune inputs. Sci. Adv. 8, eabn6240 https://doi.org/10.1126/sciadv.abn6240.

Son, M., Wang, A.G., Tu, H.-L., Metzig, M.O., Patel, P., Husain, K., Lin, J., Murugan, A., Hoffmann, A., Tay, S., 2021. NF-κB responds to absolute differences in cytokine concentrations. Sci. Signal. 14, eaaz4382. https://doi.org/10.1126/scisignal.aaz4382.

Tay, S., Hughey, J.J., Lee, T.K., Lipniacki, T., Quake, S.R., Covert, M.W., 2010. Single-cell NF-κB dynamics reveal digital activation and analogue information processing. Nature 466, 267–271. https://doi.org/10.1038/nature09145.

Unger, M.A., Chou, H.-P., Thorsen, T., Scherer, A., Quake, S.R., 2000. Monolithic microfabricated valves and pumps by multilayer soft lithography. Science 288, 113–116. https://doi.org/10.1126/science.288.5463.113.

Xue, Q., Lu, Y., Eisele, M.R., Sulistijo, E.S., Khan, N., Fan, R., Miller-Jensen, K., 2015. Analysis of single-cell cytokine secretion reveals a role for paracrine signaling in coordinating macrophage responses to TLR4 stimulation. Sci. Signal. 8 https://doi.org/10.1126/scisignal.aaa2155 ra59–ra59.

Zhou, L., Zhang, Y., Ge, Y., Zhu, X., Pan, J., 2020. Regulatory mechanisms and promising applications of quorum sensing-inhibiting agents in control of bacterial biofilm formation. Front. Microbiol. 11.

Zinski, J., Bu, Y., Wang, X., Dou, W., Umulis, D., Mullins, M.C., 2017. Systems biology derived source-sink mechanism of BMP gradient formation. Elife 6, e22199. https://doi.org/10.7554/eLife.22199.